Boron nanobelts grown under intensive ion bombardment

W. T. Li[a] and R. Boswell
Plasma Research Lab, Research School of Physical Sciences and Engineering, The Australian National University, Australian Capital Territory 0200, Australia

J. D. Fitz Gerald
Research School of Earth Sciences, The Australian National University, Australian Capital Territory 0200, Australia

(Received 2 October 2007; accepted 28 November 2007; published 3 January 2008)

High-quality α-tetragonal crystalline boron nanobelts with [001] growth axis were synthesized using a novel method combining e-beam evaporation and plasma ion bombardment techniques. Intensive ion bombardment of the growing boron nanobelts at a high substrate temperature ($\sim$1200 °C) was found to be effective in increasing the atomic density, reducing the crystal disorder, and improving the yield of the nanobelts. © *2008 American Vacuum Society.*
[DOI: 10.1116/1.2827498]

I. INTRODUCTION

Boron nanowires are of special interest, because boron has the smallest atomic weight among nonmetal solid elements, its hardness is close to diamond, and it has very high melting temperature ($\sim$2300 °C), excellent chemical inertness, and adjustable energy band gap.[1–4] These unusual features make boron nanowires attractive for various applications such as high-temperature nanoelectronic devices. Both amorphous and crystalline boron nanowires have been synthesized using different methods.[1–3] Due to high melting point and structural complexity, crystalline boron nanowires of high quality are very difficult to produce under ordinary growth conditions—high defect densities or significant disorder can be found in the crystalline boron nanowires, and the yield of the nanowires is very low.

We report a novel approach to synthesize α-tetragonal crystalline boron nanobelts (BNBs). This approach combines e-beam heating and plasma ion bombardment techniques. Both solid boron evaporant and the substrate for the BNB growth were heated by e-beam, so that the required high temperatures for the both were easily achieved. The crystalline structure and the yield of the BNBs were found to be improved greatly by applying plasma ion bombardment to the substrate.

II. EXPERIMENT

In our growth apparatus (Fig. 1), an e-beam emitted from an e-gun is divided into two sub-beams: one is launched into a carbon crucible to evaporate high-purity (99.99%) solid boron; another is directed to heat the substrate for the growth of the BNBs. The substrate was a thermally oxidized silicon wafer ($SiO_2 \sim 5$ μm thick) that was coated with a gold layer $\sim$40 nm thick to act as a catalyst. For BNB growth, the substrate was heated up to $\sim$1200 °C, and was negatively charged by the e-beam, leading to bombardment by high-density Ar ions diffused from the helicon plasma source located over the substrate. The helicon plasma was generated with Ar gas at a pressure of 1 mTorr.[5]

The general morphology of the as-grown samples was investigated using field emission scanning electronic microscopy (FESEM). The chemical composition of the BNBs was analyzed by using an energy dispersive x-ray (EDX) spectrometer attached in the FESEM. The spectra were collected from the deposited layer scraped off the original substrate onto a carbon or silicon substrate. The BNBs were also studied with a Philips CM-300 transmission electron microscope (TEM). The belts were reoriented using the TEM tilting stage to make their smallest dimension perpendicular to the electron beam, so that very clear lattice-fringe images of the belts could be obtained. The crystalline structure of the BNBs was also examined using a Philips x-ray diffraction (XRD) spectrometer (cobalt radiation $\lambda = 1.788\,97$ Å).

III. RESULTS AND DISCUSSION

Figure 2 shows the SEM and TEM images of the boron belts produced with or without helicon plasma power P. As seen from Fig. 2(a), the sample produced at $P=0$ W contains very wide boron belts or sheets (width of $\sim$0.1–1 μm, thickness of $\sim$50–100 nm), and the amount of truly nanometer-sized belts (width $<$ 100 nm, thickness $<$ 100 nm) is very small. However, the sample shown in Fig. 2(b), that was prepared at $P=600$ W, contains large amounts of very narrow belts with a width of 30–100 nm, thickness of $\sim$10–50 nm, and length from a few μm to over 15 μm. These are the real boron "nanobelts." The whole deposited mattresslike layer of the nanobelts on the substrate reached thicknesses of 1–2 mm during a deposition time of 30 min. The general yield of the BNBs at $P=600$ W was much higher than that at $P=0$ W.

Figures 2(c) and 2(e) show the low-magnification and lattice-fringe images, respectively, of a BNB typical of those prepared at $P=0$ W. This BNB has a 5–15 nm thick irregular amorphous sheath layer and a crystalline core showing stacking disorder. This kind of disorder was also observed in

[a]Author to whom correspondence should be addressed. Electronic mail: weitang.li@anu.edu.au.

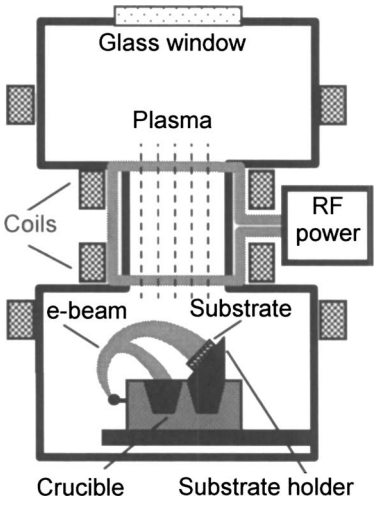

FIG. 1. Schematic of the apparatus for boron nanobelt growth.

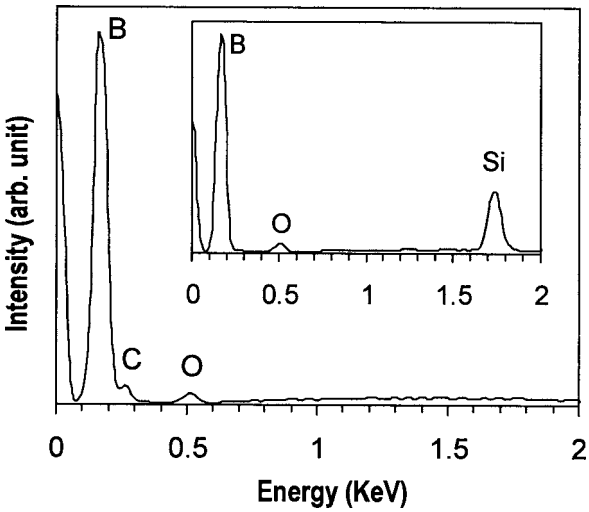

FIG. 3. Energy dispersive x-ray (EDX) spectra of the boron layer deposited at $P=600$ W and $T\sim1200$ °C. For the main spectrum, the substrate supporting the boron layer was carbon, and for the inset spectrum, it was silicon.

the BNBs produced by laser ablation.[3] In comparison, as illustrated in Figs. 2(d) and 2(f), the BNBs grown at $P=600$ W have smoother surfaces; their cores are well crystallized with uniform lattice spacing and their amorphous sheaths are only 1–3 nm thick. The lattice-fringe spacing in Fig. 2(f) is 0.44 ± 0.01 nm, which coincides well with the (200) d spacing of α-tetragonal boron (α-t-B).[6,7] The crystal c axis is always parallel to the long axis of the nanobelt.

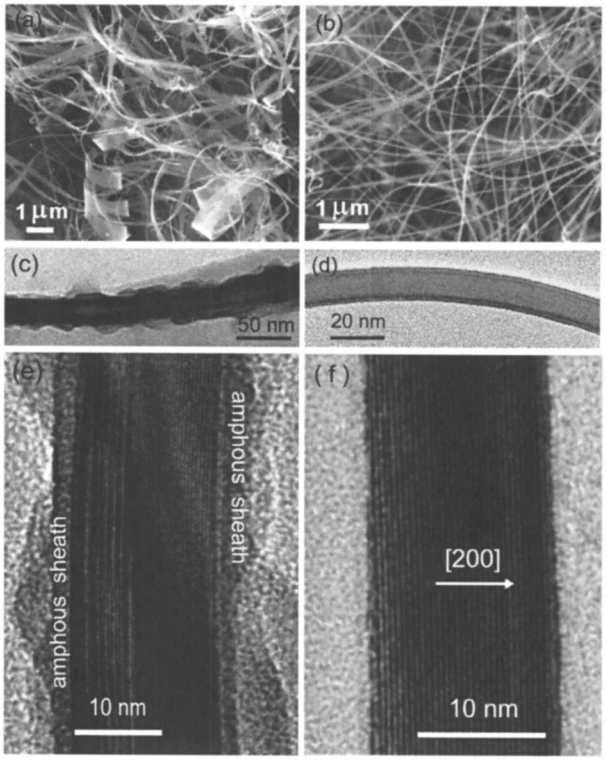

FIG. 2. (a) and (b) are SEM images of the boron deposit at helicon plasma power $P=0$ and 600 W, respectively; (c) and (d) are low-magnification TEM images of the boron belts produced at $P=0$ and 600 W, respectively; (e) and (f) are lattice-fringe TEM images of the belts produced at $P=0$ and 600 W, respectively. The substrate temperature was ~1200 °C for all these samples.

The observed differences between the two samples deposited at $P=0$ and 600 W appear to be caused by the ion bombardment. The average substrate bias voltage (V_b) was −300 V at $P=0$ W, as measured using a tungsten probe touching the substrate surface. In this case, a weak plasma was generated around the substrate due to the e-beam ionizing the background Ar gas, and thus the substrate was subjected to a weak ion bombardment. When a 600 W helicon plasma power was applied, high-density Ar^+ ions were generated and transported to the substrate resulting in the V_b changing immediately from −300 to −80 V due to faster neutralization of the electrons with ions. This indicated that the total ion flux increased dramatically although the average ion bombardment energy decreased due to the substrate bias drop. The ion bombardment is sufficiently energetic to increase the mobility of the depositing species and may also sputter away some atoms that are loosely bonded with the BNBs. These effects would be beneficial to the growth of high-quality crystalline nanobelts.

The whole deposited layer is very pure boron, except for minor oxygen contamination, as seen from the EDX spectrum in Fig. 3 of a sample deposited at $P=600$ W. The oxygen contamination may come from the surface oxidation of the BNBs, due to postdeposition exposure to air. The carbon peak in this spectrum comes from the carbon substrate, since it is not present for the Si substrate, as shown in the inset of Fig. 3. There was no Au detected in the EDX spectra of any samples, suggesting the Au catalyst might have been fully evaporated or sputtered away by the end of the deposition.

Figure 4 illustrates the typical XRD spectrum of the BNBs grown at $P=600$ W. All the major diffraction peaks can be indexed to the a-t-B in the JCPDS database (No. 75-0218: $a=8.73$ Å, $c=5.03$ Å; No. 75-0511: $a=8.75$ Å, $c=5.06$ Å).[8] It was found that the characteristic (200) peak

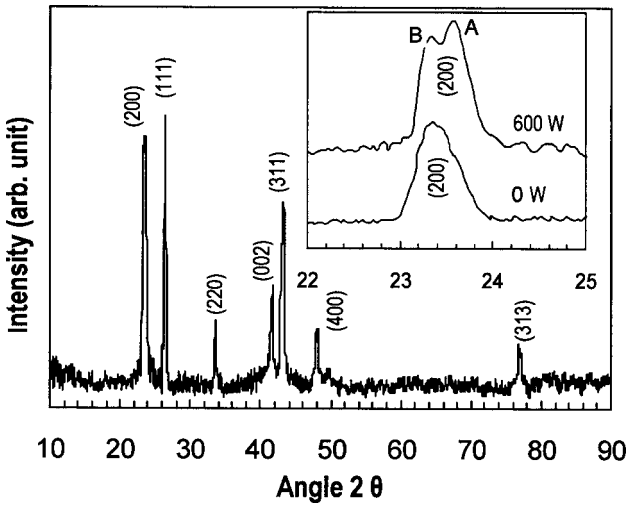

FIG. 4. Typical XRD spectrum of the boron deposit at $P=600$ W. The inset shows broadening and splitting of the (200) peak associated with applied P increase from 0 to 600 W. The two subpeaks, A and B, in the inset correspond to lattice constant a of 8.83 ± 0.01 Å and 8.74 ± 0.01 Å, respectively. The x-ray wavelength is 1.788 97 Å (cobalt radiation).

of the deposited layer shifted toward larger diffraction angle (θ) and split, if P was increased from 0 to 600 W during the BNB growth, as shown in the inset of Fig. 4. This effect is most likely caused by the generation of higher-density, less disordered boron belts under intensified ion bombardment. Low- and high-density belts may grow on the same substrate, because the ion bombardment to all the belts is not uniform due to overlapping of the belts and different orientations or locations of the belts. Therefore, the (200) peak not only broadened but also split when P was increased from 0 to 600 W.

The lattice constants of the boron belts can be determined through the well-known Bragg's equation

$$\lambda = 2d_{hkl}\sin(\theta), \tag{1}$$

where λ is the wavelength of the x ray and d_{hkl} is the space of the (hkl) planes. The resulting lattice constants for the sample deposited at $P=0$ W where $a=8.83\pm0.01$ Å, and $c=5.00\pm0.01$ Å. For the sample deposited at $P=600$ W, the lattice constants of its low-density BNBs are nearly the same as the sample deposited at $P=0$ W. Higher-density BNBs have different constants of $a=8.74\pm0.01$ Å and $c=0.503\pm0.01$ Å, which are very near the typical values of the reported large α-t-B crystals (of sizes in the micrometer to millimeter range).[6,7] It is seen here that the lattice constant a is compressed from 8.83 to 8.74 Å and thus the packing density of the boron atoms was improved when P was increased from 0 to 600 W; and the compression is mainly along the [200] direction of the BNBs, not along their growth direction [001]. (Note that such a small compression would be very difficult to directly observe in TEM lattice-fringe images.)

A tetragonal cell in the α-t-B crystals is generally believed to contain four B_{12} icosahedrons and two isolated four-coordinate B atoms, resulting in a α-t-B_{50} cell based structure.[6,7] The formation of such a-t-B_{50} crystals could be more complex and difficult than for other crystals whose basic units are the isotropic spherical atoms or ions. To form the a-t-B_{50} crystal, B_{12} icosahedra units may grow first; then, the B_{12} units organize with linking B atoms to form the a-t-B_{50} cells and, subsequently, bulk crystal. Formation of the B_{12} icosahedrons could be very easy, since they were found to be the basic units in all amorphous and crystalline boron.[6,7] The assembly of the B_{12} units into the a-t-B_{50} unit cells and into bulk crystal are probably relatively difficult processes, due to the relatively large dimension of the B_{12} units and their anisotropic nature. Stacking disorder or faults are thus easily generated in the a-t-B_{50} crystals, as commonly observed in the micrometer-to millimeter-sized a-t-B_{50} crystals,[6] and in our BNBs deposited at $P=0$ W. Similar to diamond, the growth of perfect a-t-B_{50} crystals may require very high temperature and high pressure or suitable ion bombardment, as demonstrated by the growth of the BNBs under high-power ion bombardment.

IV. CONCLUSIONS

In summary, α-t-B nanobelts were synthesized using a novel method combing e-beam evaporation and plasma ion bombardment techniques. It was shown that ion bombardment plays a key role in increasing the atomic density, reducing defects and disorder, thinning the amorphous sheath layers, and improving the yield of the boron nanobelts.

ACKNOWLEDGMENTS

This work was supported by the Australian Research Council (ARC). The authors thank Hua Chen for his assistance on XRD measurements.

[1]S. H. Yun, J. Z. Wu, A. Dibos, X. Gao, and U. O. Karlsson, Appl. Phys. Lett. **87**, 113109 (2005).
[2]K. Kirihara, Z. Wang, K. Kawaguchi, Y. Shimizu, T. Sasaki, N. Koshizaki, K. Soga, and K. Kimura, Appl. Phys. Lett. **86**, 212101 (2005).
[3]Z. Wang, Y. Shimizu, T. Sasaki, K. Kawaguchi, K. Kimura, and N. Koshizaki, Chem. Phys. Lett. **368**, 663 (2003).
[4]S. H. Yun, J. Z. Wu, A. Dibos, X. Zou, and U. O. Karlsson, Nano Lett. **6**, 385 (2006).
[5]W. T. Li, D. A. P. Bulla, C. Charles, R. Boswell, J. Love, and B. Luther-Davies, Thin Solid Films **419**, 82 (2002).
[6]J. L. Hoard, R. E. Hughes, and D. E. Sands, J. Am. Chem. Soc. **73**, 4507 (1958).
[7]D. Li, Y. N. Xu, and W. Y. Ching, Phys. Rev. B **45**, 5895 (1992).
[8]JCPDS-International Center for Diffraction Data, PCPDFWIN, V.2.02, 1999.